Fall 2011

Impact of channel statistics and correlation on underwater acoustic communication systems

Jesse Scott Cross

Department:

IMPACT OF CHANNEL STATISTICS AND CORRELATION ON UNDERWATER ACOUSTIC COMMUNICATION SYSTEMS

by

JESSE SCOTT CROSS

A THESIS

Presented to the Faculty of the Graduate School of the

MISSOURI UNIVERSITY OF SCIENCE AND TECHNOLOGY

in Partial Fulfillment of the Requirements for the Degree

MASTER OF SCIENCE IN ELECTRICAL ENGINEERING

2011

Approved by

Dr. Yahong Rosa Zheng
Dr. Chengshan Xiao
Dr. Steven Grant

PUBLICATION THESIS OPTION

This thesis contains papers published in the style used by the Navy Journal of Underwater Acoustics (NJUA) and in the style used by the IEEE Military Communications Conference (MILCOM). Pages 3-19 have been published in the NJUA in 2010. Pages 20-32 have been published in MILCOM 2010 and pages 33-45 are accepted for publication in MILCOM 2011.

ABSTRACT

Several statistical properties of underwater acoustic channels gathered from experiment data are analyzed. The baseband channel impulse response (CIR) is estimated using a time domain least squares technique with a sliding window applied to the probing sequences. From the CIR estimation, the probability distribution functions (PDFs) of the magnitude, real part, imaginary part, and phase of the CIR are calculated. Gamma, Rayleigh, and compound k distributions are fitted to the magnitude PDF and the fitness of the distributions are calculated with a two-sample Kolmogorov-Smirnov test. Other statistics such as the autocorrelation function, coherence time, and scattering function are evaluated. The results show that the underwater acoustics channels are worse than the Rayleigh fading commonly seen as the worst case radio channel.

Furthermore, the spatial and intertap correlation matrices of multiple input multiple output (MIMO) systems are estimated using experimental data. It is shown that underwater acoustic MIMO channels exhibit high spatial and temporal correlation. The bit error rate (BER) of the receiver using Frequency-domain turbo equalization is also evaluated in different channel correlation setups, demonstrating strong effects of the spatial-temporal correlation function on the performance.

ACKNOWLEDGMENTS

I would like to extend my gratitude toward all who have helped me achieve my master's degree.

First, I would like to thank my mother and all the rest of my family members for their support while I worked toward my master's degree.

I would like to thank Dr. Yahong Rosa Zheng for her guidance throughout my time at MS&T, for the undergraduate student research position from June 2007 to May 2010, and for the graduate research position starting from June 2010 to Dec. 2011. I would also like to thank Dr. Chengshan Xiao and Dr. Steven Grant for being a part of my master's degree committee. I would like to thank Jian Zhang for his help with the papers included in this thesis.

I would like to express my gratitude for the chancellor's fellowship. I am grateful for the support provided by the Intelligent Systems Center. The papers included in this thesis were supported in part by the National Science Foundation under Grant ECCS-0846486 and the Office of Naval Research under Grants N00014-10-1-0174.

TABLE OF CONTENTS

SECTION

LIST OF ILLUSTRATIONS

LIST OF TABLES

1. INTRODUCTION

Underwater acoustic (UWA) channels have a much longer range (1 km – 1000 km) than underwater radio channels; however, underwater acoustic channels are much more severe and present many additional challenges such as excessive path loss, a complicated propagation paths, and a time-varying nature. Statistical analysis of in-air radio frequency (RF) channels is already established. In the past, most modeling of underwater acoustic channels has focused on wave propagation with limited statistical analysis. Recent ocean experiments have shown that the UWA channels exhibit worse than Rayleigh fading and an extreme Doppler shift in comparison to the carrier frequency. The long multipath delay time results in severe intersymbol interference (ISI) and a channel impulse response (CIR) that has many more taps than an RF system. All of these properties result in the need to re-estimate the channel repeatedly which increases the computational complexity of an underwater communication system as compared to an RF system.

The papers presented in this thesis analyze data gathered in three ocean experiments. The first is Reschedule Acoustic Communication Experiment (RACE) conducted in Narragansett Bay, Rhode Island, March 2008; the second is the ACOMM experiment conducted in New Jersey in 2009 (ACOMM09); and the third is the Surface Process and Acoustic Communications Experiment conducted in fall 2008 (SPACE08) by the Woods Hole Oceanographic Institute (WHOI). Data from these experiments are used to investigate the statistical characteristics of UWA channels, including the probability density function (PDF), autocorrelation function, crosscorrelation function, and scattering function of the baseband equivalent CIRs. A sliding window least squares technique is used to estimate and track the time-varying CIRs. Various theoretical PDFs are fitted to the estimated CIR PDF and the Kolmogorov-Smirnov test is used to quantize the level of fitness. The effects of spatial correlation on the bit error rate (BER) are investigated. Trials with differing amounts of receivers but with equal aperture are run. A simulation is conducted to confirm the experimental results are due to spatial correlation. The

Kronecker properties of the spatial correlation matrix are analyzed. The matrix is decomposed into a series of Kronecker products and the error resultant matrix formed by the decomposed matrices and the original matrices is quantified.

It is shown that the experimental PDF matches the compound k distribution. The compound k distribution presents additional challenges over the Rayleigh distribution of in air RF channels. Since the taps follow the compound k distribution rather than the Rayleigh distribution, there is a much larger probability that the channel tap will be low while at the same time there is an equal probability that the tap will be large. This necessitates a receiver with a much larger dynamic response so that the receiver has a good response with low tap values but does not become saturated with high tap values. The channel coherence time of the channels analyzed is shown to be about 470 symbol periods long. This implies that the receiver must use data blocks smaller than this in order to have an invariant channel during the transmission of the data block. When the number of receivers is reduced while maintaining a constant aperture, the BER remains relatively constant. This shows spatial correlation plays a large part in receiver placement.

PAPER

1. Statistical Properties of Multiple-Input Multiple-Output (MIMO) Underwater Acoustic Communications Channels

Jesse Cross[1], Jian Zhang[2], and Yahong Rosa Zheng[1]

[1]Department of Electrical and Computer Engineering,

Missouri University of Science and Technology, Rolla, MO 65409

[2] now at Broadcom Corp., San Diego, CA 92127

Abstract

Statistical characteristics of underwater acoustic channels are estimated by ocean experimental data obtained in the RACE08 and ACOMM09 experiments. First, base-band complex channel impulse responses (CIRs) are estimated by a time-domain least square method with sliding windows applied to long probing sequences. Second, the statistics of the CIRs are analyzed, including the probability density functions (PDF) of the real and imaginary parts and of the magnitude and phase, autocorrelation functions, channel coherence time, and scattering function. Spatial correlation of multiple transducers and hydrophones are also extracted for multiple-input multiple-output (MIMO) channels.

1.1. Introduction

Underwater acoustic (UWA) propagation is proven to be the effective means of underwater wireless communication for medium and long ranges (1 km – 1000 km). However, underwater acoustic channels, especially shallow water horizontal channels, are often more challenging than radio frequency (RF) channels due to excessive path loss, complicated propagation environment, and time-varying inhomogeneous media. Statistical modeling of RF channels has been well established in the literature and has played important roles in capacity analysis, transceiver design, and performance evaluation.

However, analysis and modeling of UWA channels focused on the acoustic wave propagation mechanism in the past and limited studies are available for extracting statistical properties [1, 2].

Extensive ocean experiments have been conducted over the past two decades and existing UWA channel statistics studies show that UWA channels are often worse than Rayleigh fading, which in turn heavily impacts the bit error rate (BER) performance [4]. Multipath and Doppler effect of UWA are described in [1, 2] providing guidelines in equalizer design. Wideband UWA channel is modeled in [5] recently. It is shown that UWA channel capacity is also greatly impacted by accurate channel models [6].

This paper analyzes ocean experiment data collected in the Reschedule Acoustic Communication Experiment (RACE), Narragansett Bay, Rhode Island, March 2008, and the data collected in the ACOMM09 experiment conducted in New Jersey in 2009 (ACOMM09). This paper also investigates the statistical characteristics of UWA channels, including the probability density function (PDF), autocorrelation function, cross-correlation function, and scattering function of the baseband equivalent channel impulse responses (CIRs). The complex CIRs are estimated by a sliding window least square method, where small window length and sliding width are used for long probing data sequences to accurately track the time-varying CIRs. The Kolmogorov-Smirnov (KS) test [7] is employed to statistically test the fitness between the PDF of estimated CIRs and theoretical PDFs. The test results show that the experimental channel magnitude PDF matches the compound K distribution with small shape parameters. This results complement previous investigation in wireless RF [8, 9] and underwater [4, 10] channels. Our results also show that the phases of CIRs are approximately uniform in $[0, 2\pi]$ and the autocorrelation function exhibits exponential decay that is dominated by the Gamma component of the compound K distribution. The channel scattering function is obtained from the correlation function providing channel characteristics in the delay-Doppler plane.

These statistical properties provide design guidelines for channel estimation, channel equalization, pilot insertion, and transceiver signaling.

1.2. Channel model and channel statistics

Consider first a single-input single-output communication system with one transducer and one hydrophone. Let $\tilde{s}(t)$ denote the baseband equivalent complex signal and $S(t) = \mathrm{Re}\{\tilde{s}(t)e^{j2\pi f_c t}\}$ denote the passband transmit signal with a carrier frequency f_c. At the receiver, the received signal is $R(t) = \mathrm{Re}\{\tilde{r}(t)e^{j2\pi f_c t}\}$, where $\tilde{r}(t)$ is baseband complex envelop. Then $\tilde{r}(t)$ can be represented as

$$\tilde{r}(t) = \int h(t,\tau)\tilde{s}(t-\tau)d\tau \tag{1.1}$$

where $h(t,\tau)$ is the equivalent complex baseband impulse response for a time-varying frequency-selective channel. In a multipath and Doppler spread propagation environment, we assume there are I multi-paths and each path has distinguished delay and Doppler shift. Then, the channel impulse response is modeled as

$$h(t,\tau) = \sum_{i=1}^{I} A_i \cdot e^{j2\pi(f_{d,i}t - f_{d,i}\tau_i - f_c\tau_i)} \cdot \delta(\tau - \tau_i) \tag{1.2}$$

where A_i, τ_i, and $f_{d,i}$ are the gain, propagation delay, and instantaneous Doppler shift at the i-th path. Although acoustic communication channels are time varying resulting in time-varying A_i, τ_i, and $f_{d,i}$, the time variation is very small within the channel coherence time, thus these parameters are usually assumed to be constant in a short time interval. Therefore we drop the dependence of the channel impulse response with respect to t and denote $h(\tau)$ as the so called quasi-static channel.

Next, consider a MIMO communication system with N_t transducers and N_r hydrophones. Denote $h_{m,n}(l)$ the subchannel CIR linking the m-th hydrophone with the n-th transducer with sampling at the symbol duration T_s, where $l = 1, 2, \cdots, L$. The

MIMO channel is represented by the channel matrix

$$\mathbf{H}(l) = \begin{bmatrix} h_{1,1}(l) & h_{1,2}(l) & \cdots & h_{1,N_t}(l) \\ \vdots & \vdots & \ddots & \vdots \\ h_{1,1}(l) & h_{1,2}(l) & \cdots & h_{N_r,N_t}(l) \end{bmatrix}, \tag{1.3}$$

and the input-output relationship of the MIMO system is then

$$\mathbf{r}(k) = \sum_{l=1}^{L} \mathbf{H}(l)\mathbf{s}(k-l) + \mathbf{w}(k), \tag{1.4}$$

where k is the time index, transmitted, received, and noise vectors are respectively $\mathbf{s}(k) = [\tilde{s}_1(k) \cdots \tilde{s}_{N_t}(k)]^T$, $\mathbf{r}(k) = [\tilde{r}_1(k) \cdots \tilde{r}_{N_r}(k)]^T$, and $\mathbf{w}(k) = [w_1(k) \cdots w_{N_r}(k)]^T$, with superscript T denoting transpose.

1.2.1. Channel Estimation. A time-domain least squares (LS) method is employed in this paper to probe the channel impulse response (CIR) from the baseband input and output signals. A long probing sequence is transmitted by the transducer and the CIRs are estimated progressively by using a sliding window of size N_p.

Let $\mathbf{s}_n^p$ denote the probing symbols of the n-th transducer at the p-th step. The estimated time-domain CIR for the m-th hydrophone is $\hat{\mathbf{h}}_m^p = [(\hat{\mathbf{h}}_{m,1}^p)^T, \cdots, (\hat{\mathbf{h}}_{m,N_t}^p)^T]^T$, where $\hat{\mathbf{h}}_{m,n} = [\hat{h}_{m,n}^s(1), \cdots, \hat{h}_{m,n}^s(L)]^T$ with a channel length L and N_t is the number of transducers, can be estimated as

$$\hat{\mathbf{h}}_m^p = (\mathbf{s}^p)^\dagger \cdot \mathbf{r}_m^p \tag{1.5}$$

where $()^{\dagger}$ denotes the pseudo inverse, $\mathbf{r}_m^p = [r_m^p(L), \cdots, r_m^p(N_p)]^T$ which is the corresponding MIMO channel output vector, and $\mathbf{s}^p = [\mathbf{T}_1^p | \cdots | \mathbf{T}_{N_t}^p]$ with

$$\mathbf{T}_n^p = \begin{bmatrix} s_n^p(L) & s_n^p(L-1) & \cdots & s_n^p(1) \\ s_n^p(L+1) & s_n^p(L) & \cdots & s_n^p(2) \\ \vdots & \ddots & \ddots & \vdots \\ s_n^p(N_p) & s_n^p(N_p-1) & \cdots & s_n^p(N_p-L+1) \end{bmatrix} \tag{1.6}$$

where $n = 1, \cdots, N_t$. Let N_d denote the sliding step of the data window. The CIR is re-estimated every $N_d T_s$ interval, where T_s is the symbol period.

1.2.2. Magnitude Distributions. Let X have a Rayleigh distribution with a parameter σ, then the conditional PDF of X is given as

$$f_X(x) = \frac{x}{\sigma^2} \exp\left(-\frac{x^2}{2\sigma^2}\right) \tag{1.7}$$

The PDF of a Gamma distributed X is given as

$$f_X(x) = \frac{1}{b^a \Gamma(a)} x^{a-1} \exp\left(-\frac{x}{b}\right) \tag{1.8}$$

where $\Gamma(\cdot)$ is the Euler gamma function and a and b are scalar parameters.

The unconditioned PDF of X, if X has a compound K distribution, is given as

$$f_X(x) = \frac{4}{\sqrt{\beta}\Gamma(\nu)} \left(\frac{x}{\sqrt{\beta}}\right)^{\nu} K_{\nu-1}\left(\frac{2x}{\sqrt{\beta}}\right) \tag{1.9}$$

where $K_{\nu-1}$ is the modified bessel function of the second kind of order $\nu - 1$. A Rayleigh distribution results when $v \to \infty$ and $\beta\nu = 2\sigma^2$ remains constant. Therefore, as ν decreases the channel gets worse than Rayleigh fading.

The first and second moments were used to fit the PDFs of the different distributions to the measured data and are given in the Table 1.1.

Table 1.1 The first and second moments of Rayleigh, Gamma, and Compound KDistributions

	Rayleigh	Gamma	Compound K
$E(x)$	$\sigma\sqrt{\frac{\pi}{2}}$	ab	$\frac{\sqrt{\beta\pi}}{2} \cdot \frac{\Gamma(\nu+0.5)}{\Gamma(\nu)}$
$E(x^2)$	$\frac{4-\pi}{2}\sigma^2$	ab^2	$\beta\nu$

1.2.3. Kolmogorov-Smirnov (KS) Test. The KS test is one of the most useful and general nonparametric tools to quantify the similarity of two empirical distribution functions. The two-sample KS test can serve as a goodness of fit test, and is used to determine if two datasets share a common probability distribution. No assumptions are made about the distributions of the two datasets. The null hypothesis of the KS test is that both datasets do not differ significantly and therefore follow the same distribution. The alternative hypothesis is that the two datasets follow different distributions. The Kolmogorov-Smirnov statistic D is defined as [7]

$$D_{n,n'} = \sup_x |F_n(x) - F_{n'}(x)| \tag{1.10}$$

where $F_n(x)$ and $F_{n'}(x)$ are the empirical cumulative distribution functions (CDF) of the two distributions to be compared and sup is the supremum of the set $|F_n(x) - F_{n'}(x)|$.

The alternative hypothesis will be accepted at level α if

$$Q_\alpha < D_{n,n'}\sqrt{\frac{nn'}{n+n'}} \tag{1.11}$$

where Q_α is found by $P(Q \leq Q_\alpha) = 1 - \alpha$ and Q is a Kolmogorov distributed random variable; n and n' are the number of samples in the compared distributions, respectively.

1.2.4. Channel Scattering Function. Generally, the channel impulse response $h(t, \tau)$ is considered as a two-dimensional random process for frequency selective channels.

The general second-order autocorrelation function of $h(t,\tau)$ can be written as

$$R_h(t_1,t_2;\tau_1,\tau_2) = \mathrm{E}[h(t_1,\tau_1)h^*(t_2,\tau_2)]. \tag{1.12}$$

where E() denotes statistical expectation. To simplify this four-dimensional correlation function, we make an assumption that the channel is wide sense stationary in the short term, *i.e*, the second-order statistics depends only on the difference between time instants, rather than the absolute time. Therefore, the autocorrelation of $h(t,\tau)$ is simplified as

$$\mathrm{E}(h(t+\Delta t,\tau_1)\cdot h^*(t,\tau_2)) = R_h(\Delta t,\tau_1)\delta(\tau_1-\tau_2) \tag{1.13}$$

and the channel scattering function is defined by [11]

$$S(f,\tau) = \int_{-\infty}^{\infty} R_h(\Delta t,\tau)e^{-j2\pi f\Delta t}d\Delta t \tag{1.14}$$

The two-dimensional scattering function (1.14) depicts the power spectral density of the channels along geo-time and completely describes the second-order statistics of a stationary fading channel.

1.3. Experimental results

The underwater experiment, named as Reschedule Acoustic Communication Experiment (RACE), was conducted in Narragansett Bay, Rhode Island, by Woods Hole Oceanographic Institution (WHOI), in March 2008. The water depth varied between 9 to 14 meters. The transmitter with an array of two transducers was fixed on a tripod and was four meters above the sea bottom. The receiver with an array of 12 hydrophones was also fixed on a tripod and was located two meters above the sea bottom. In this study, the data was collected when the distance between the transmitter and receiver was 1000 meters. The carrier frequency was $f_c = 11.5$ kHz, the sampling rate $f_s = 39.0625$ kHz, and the bandwidth $B = f_s/10 = 3.90625$ kHz.

A probing sequence with a duration of 22 seconds was transmitted to probe the channel impulse responses. A sliding window was used with a window size $N_p = 128$ and the interval between adjacent window $N_d = 32$. Hence, the sampling rate at the absolute time domain is $1/(32 \cdot T_s) = 122$ Hz which means the channels are estimated in every 8.2 milliseconds. The channel impulse responses (CIRs) were estimated progressively by the LS method described in (1.5). For each tap, 2144 samples were obtained in one probing data packet. The two-dimensional time-varying CIRs for the subchannel corresponding to (Tx1, Rx1) and (Tx2, Rx1) are plotted in Fig. 1.1(a) and Fig. 1.1(b). The frequency-selective channel length spans 25 symbol periods.

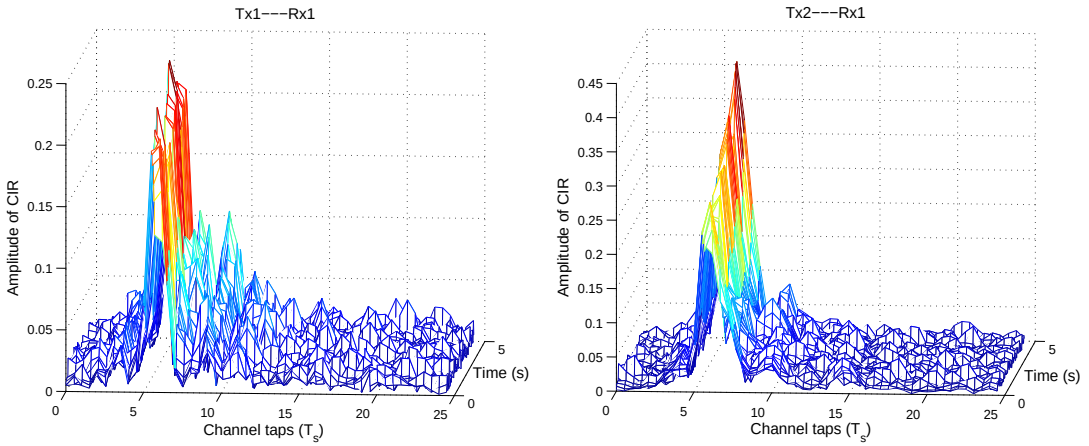

(a) Estimated CIRs for the subchannel Tx1—Rx1

(b) Estimated CIRs for the subchannel Tx2—Rx1

Figure 1.1 Estimated time-varying frequency-selective channel impulse responses in the RACE08 experiment.

The ACOMM09 was conducted by Naval Research Laboratory (NRL) at the coastline of New Jersey in May 2009. The symbol period was 0.2 ms and the carrier frequency was 17 kHz. Modulations included QPSK (Quadrature Phase Shift Keying), 8-PSK, and 16-QAM (Quadrature Amplitude Modulation). The transmit array consisted of two transducers located at 25 $\sim$ 75 m deep from the sea surface. Two receive hydrophone arrays, ACDS2 and ACDS3, were deployed, with their distances to the transmitter being

2 km and 3 km, respectively. The depths of ACDS2 and ACDS3 were 20 $\sim$ 34.4 m and 40 $\sim$ 54.4 m, respectively. Each hydrophone array consisted of eight hydrophones with the inter-hydrophone spacing being 2.06 m.

The channel length was measured as $L = 200$ in this experiment. An example of the estimated channels for two-transducer transmission, as shown in Fig. 1.2, demonstrated that the two transmitter channels were unbalanced with Tx2 having approximately half of the power as those of Tx1. The CIR of Tx2-Rx4, for example, was also non-minimum phase which may cause significant difficulties in channel synchronization and equalization.

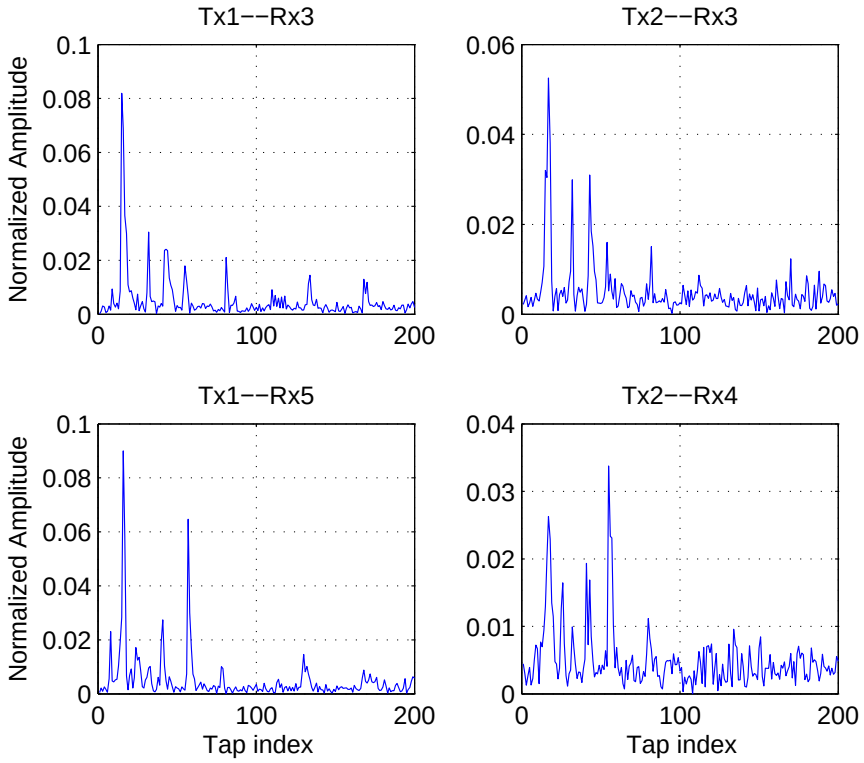

Figure 1.2 Estimated channel impulse responses in ACOMM09 experiment.

Figures 1.3(a) and 1.3(b) show the real and imaginary parts of the RACE08 measured data distribution versus a Gaussian distribution with the same mean and different

variances. Fig. 1.4(a) and Fig. 1.4(b) show the measurements for ACOMM09. We can see the measured PDFs of the real and imaginary parts do not follow the Gaussian distribution. For the probability densities around large values, the Gaussian distribution with large variance matches the tails of the measured PDFs. However, for the probability densities at small values, the Gaussian distributions with small variance fit the peaks of the measured PDFs better.

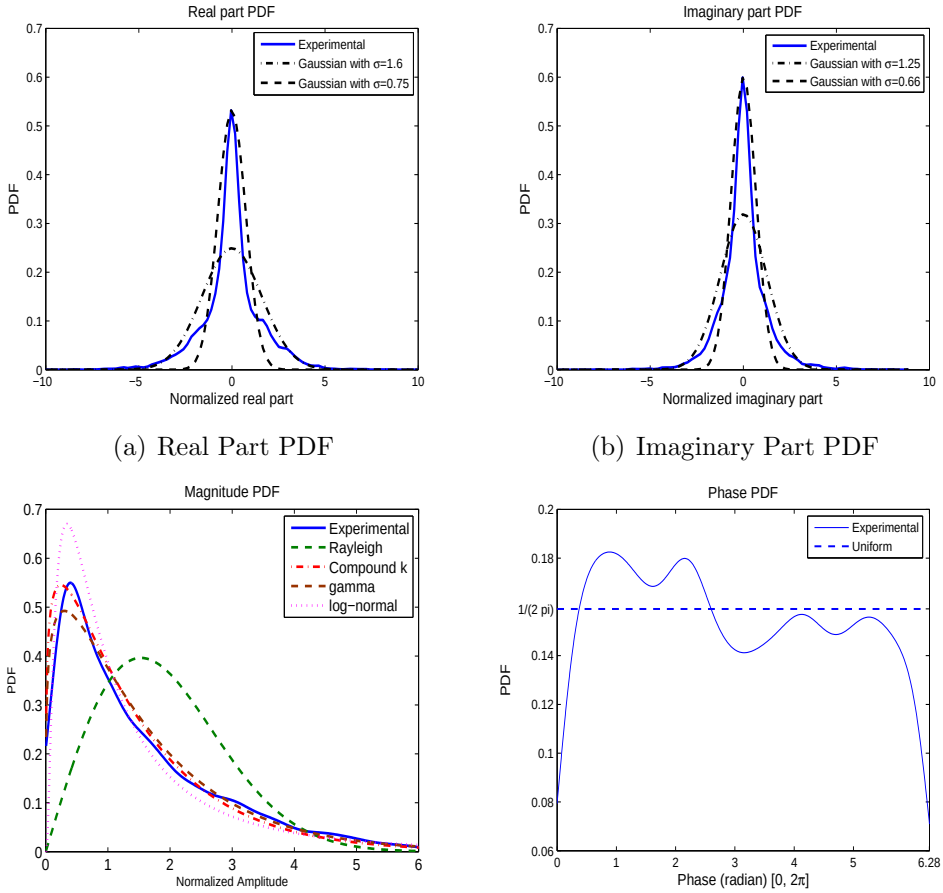

(a) Real Part PDF

(b) Imaginary Part PDF

(c) Magnitude PDF

(d) Phase PDF

Figure 1.3 The PDFs of the RACE08 complex CIR. (a) PDF of real part versus Gaussian with $\sigma = 1.6$ and 0.75. (b) PDF of imaginary part versus Gaussian with $\sigma = 1.25$ and 0.66. (c) PDF of magnitude versus compound Kand other distributions. (d) PDF of phase versus uniform distribution.

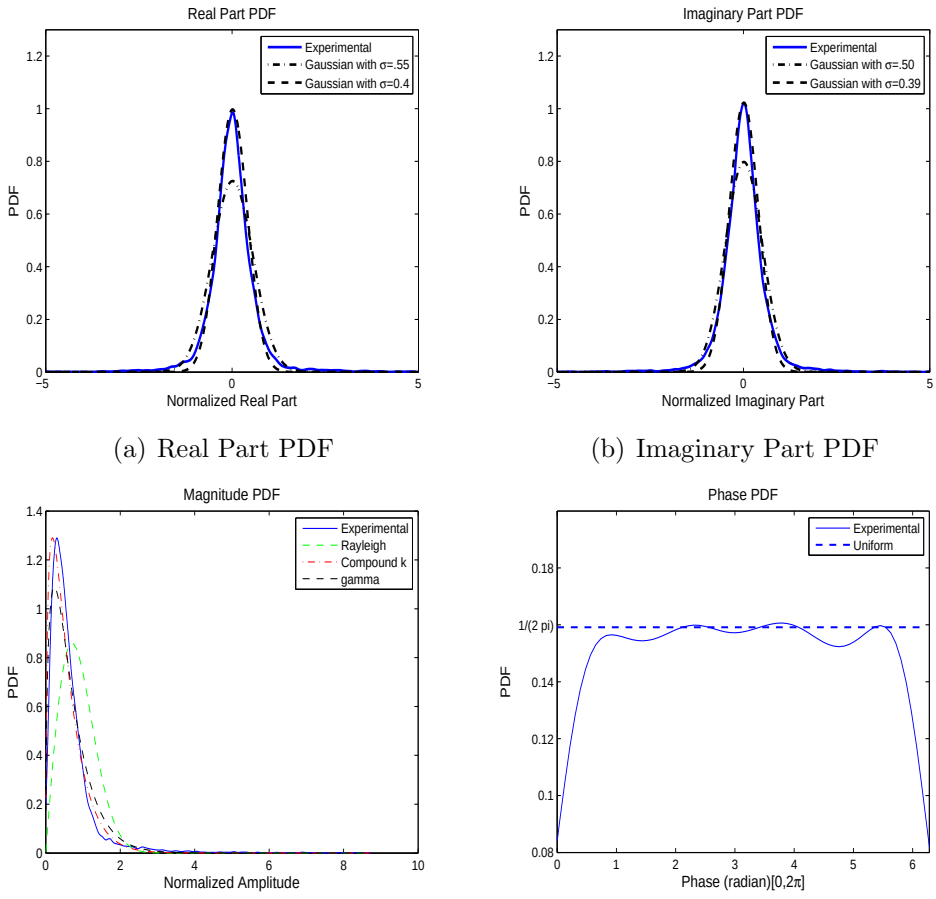

(a) Real Part PDF (b) Imaginary Part PDF

(c) Magnitude PDF (d) Phase PDF

Figure 1.4 The PDFs of the ACOMM09 complex CIR. (a) PDF of real part versus Gaussian with $\sigma = 0.55$ and 0.40. (b) PDF of imaginary part versus Gaussian with $\sigma = 0.50$ and 0.39. (c) PDF of magnitude versus compound Kand other distributions. (d) PDF of phase versus uniform distribution.

Since the real and imaginary parts are not well represented by Gaussian distributions, it is reasonable to predict the magnitude probability distribution will not follow a Rayleigh distribution. Fig. 1.3(c) shows the RACE08 measured magnitude PDF versus fitted compound Kand other distributions. Fig. 1.4(c) shows the same for the ACOMM09 experiment. It can be seen visually that the Rayleigh and Gamma distributions are not a good fit. The KS test was used to compare the measured PDF with different distributions to find the best match to the measured PDF. The KS test results for different distributions are depicted in Table 1.2. The p-value represents the probability of a test

Table 1.2 The Kolmogorov-Smirnov results for the measured PDF when compared to different fitted distributions

		Gamma	Rayleigh	Compound K
RACE08	Parameters	$a = 1.065, b = 0.8$	$\sigma = 0.70$	$\nu = 0.63, \beta = 6.04$
	p-value	1.18×10^{-6}	1.1×10^{-51}	0.96
	$D_{n,n'}$	0.16	0.48	0.07
	Results	reject	reject	accept
ACOMM09	Parameters	$a = 1.05, b = 0.4$	$\sigma = 0.4$	$\nu = 1.25, \beta = 0.42$
	p-value	1.10×10^{-7}	1.0×10^{-50}	0.1196
	$D_{n,n'}$	0.7646	0.7546	0.0392
	Results	reject	reject	accept

statistic at extreme as the one actually observed. If the significance level $\alpha = 5\%$, the null hypothesis is rejected when the p-value is less than 0.05. The $D_{n,n'}$ is the maximum distance between two CDFs, and the results have two choices: reject or accept the null hypothesis. The fit test parameters for different distributions were chosen from the KS test that returned the highest p-value. For the RACE08 data, the null hypothesis that the measured distribution follows the fitted compound Kdistribution with $\nu = 0.63$ and $\beta = 6.04$ was accepted with a p-value of 0.96 and $D_{n,n'} = 0.07$. However, the null hypothesis that the measured data is subject to the best fit Rayleigh distribution was rejected with a very small p-value, 1.1×10^{-51}. The null hypothesis that the measured channel followed the fitted Gamma distribution was rejected with a p-value of 1.18×10^{-6}. Therefore, we conclude that the measured data follows a compound Kdistribution rather than a Rayleigh or Gamma distribution for the RACE08 channel. Similarly, the ACOMM09 measured channel also followed a compound K distribution with $\nu = 1.25$ and $\beta = 0.42$, as shown in Table 1.2.

The normalized autocorrelation functions of each channel tap for real part, imaginary part and complex envelop are depicted in Fig. 1.5. It is noted that these three autocorrelation curves behave similarly all with exponential decay. Define the channel coherence time as the time over which the autocorrelation is above 0.5. The coherence time was approximately $T_c = 0.12$s for this channel. It implies that the channel can

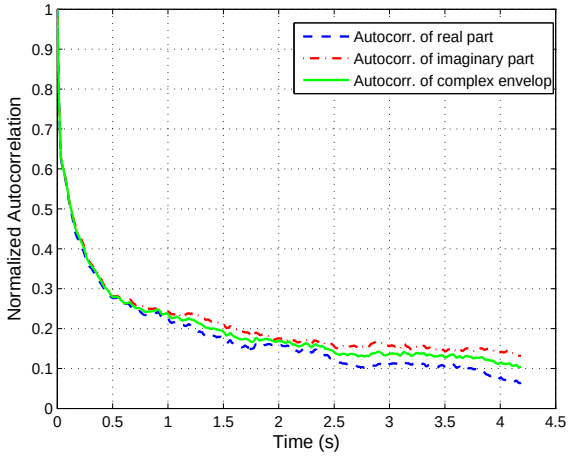

Figure 1.5 The normalized autocorrelation of the real part, imaginary part, and complex envelop of the CIR. The autocorrelation function was dominated by the Gamma component of the CIR. The coherence time of the channel was about 120 ms.

be considered to be invariant if the length of data block is less than $T_c \cdot B \approx 470$ symbols. The relation between the coherence time and the maximum Doppler spread is given by [12]

$$T_c \approx \frac{9}{16\pi f_m} \tag{1.15}$$

where f_m is maximum Doppler shift. In this case, $f_m = 1.5$ Hz and the dynamic range of the instantaneous Doppler spread is $[-1.5, 1.5]$ Hz. Figure 1.6 shows the cross correlation of the real and imaginary part of the CIR. It is seen that the real parts and the imaginary part are uncorrelated.

The spatial correlation between hydrophone Rx1 and the other hydrophones is presented in Fig. 1.7 for the RACE08 channel, where Rx 1 was the hydrophone located at the very bottom of the vertical array and Rx12 was the one at the top of the array. Define the coherence distance as the distance away from Rx1 where the spatial correlation is above 0.5. It is clear from the figure that within the channel coherence time $120ms$, the spatial correlation between Rx1 and Rx2 was above 0.5, thus the two receive hydrophones were spaced within the coherence distance. The spatial correlation between Rx 1 and

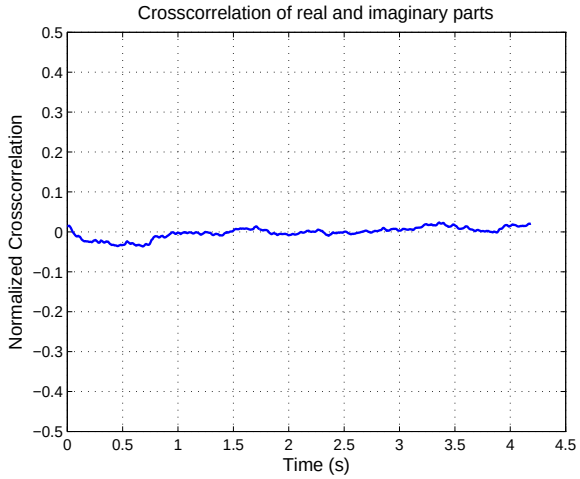

Figure 1.6 The normalized cross correlation between the real and imaginary parts of the CIR. The real and imaginary parts were uncorrelated.

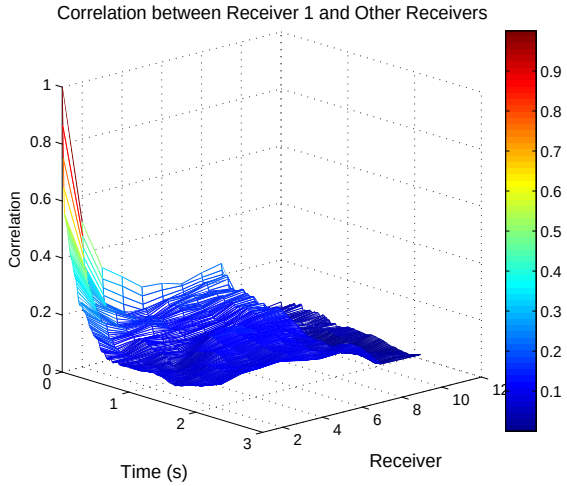

Figure 1.7 The normalized spatial correlation between Rx1 and the other hydrophones for RACE08 channel. The normalized correlation was averaged across the 25 taps.

other hydrophones were all below 0.5 and can be considered as spatially uncorrelated. The spatial correlation between other pairs of hydrophones exhibited similar results as being correlated if spaced within coherent distance and uncorrelated if spaced far apart. The figures are not shown here for brevity.

The two-dimensional scattering function is shown in Fig. 1.8 by performing Fourier transform on the correlation function. We see that the average Doppler shift is very small, close to zero Hz since the transceiver platforms were always fixed during the experiment and the motion of the wave was not significant. From the power spectral density, the channel has a Doppler spread of $[-1.5, 1.5]$ Hz at a delay of $1 \sim 2.5$ ms.

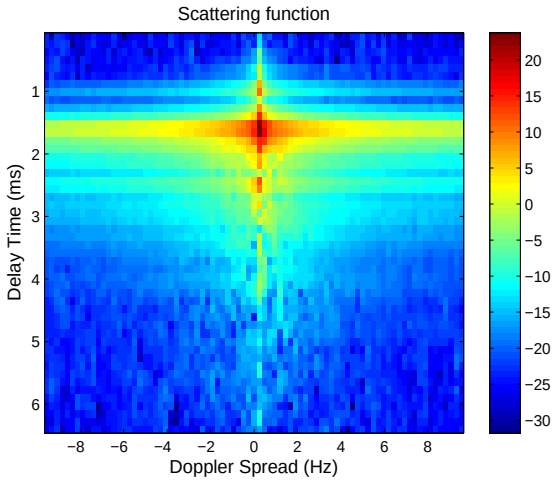

Figure 1.8 The channel scattering function of the RACE08 experiment.

1.4. Conclusion

In this paper, we presented the statistical characteristics, including PDF and second-order statistics, for the UWA channels measured in RACE08 and ACOMM09 ocean experiments. Experimental results demonstrate that the real and imaginary parts of the complex UWA channels do not follow Gaussian; the PDF of the magnitude fits the compound K distribution; the PDF of phase approximately follows uniform distribution. The autocorrelations of CIRs behave like decaying exponential curves and the channel coherence time is also roughly estimated. The very low spatial correlation between the

receivers has a profound impact on the design of MIMO systems. The scattering function provides better understanding on the spectral density of the UWA channels.

1.5. Acknowledgment

This work was supported in part by the National Science Foundation under Grant ECCS-0846486 and the Office of Naval Research under Grants N00014-10-1-0174. The authors are grateful to Dr. J. Preisig of WHOI and Dr. T. C. Yang of NRL for their leadership in conducting the RACE08 and ACOMM09 experiments, respectively.

References

[1] M. Stojanovic and J. Preisig, "Underwater acoustic communication channels: propagation models and statistical characterization," *IEEE Commun. Mag.*, pp.84-89, Jan. 2009.

[2] A. C. Singer, J. K. Nelson, S. S. Kozat, "Signal processing for underwater acoustic communications," *IEEE Commun. Mag.*, pp.90-96, 2009.

[3] W. Yang and T. C. Yang, "High frequency channel characterization for M-ary frequency-shift keying underwater acoustic communications," *J. Acoust. Soc. Am.*, vol.120, pp.2615-2626, Nov. 2006.

[4] W. Yang and T. C. Yang, "M-ary frequency shift keying communications over an underwater acoustic channel: performance comparison of data with models," *J. Acoust. Soc. Am.*, vol.120, pp.2694-2701, Nov. 2006.

[5] A. G. Zajić, "Statistical space-time-frequency characterization of MIMO shallow water acoustic channels," in *Proc. IEEE OCEANS'09*, Bloxi, MS, USA, Oct. 26-29, 2009.

[6] T. J. Hayward and T. C. Yang, "Single-and multi-channel underwater acoustic communication channel capacity: A computational study," *J. Acoust. Soc. Am.*, vol.22, pp.1652-1661, Sep. 2007.

[7] F. J. Massey, "The Kolmogorov-Smirnov test for goodness of fit," *J. Am. Stat. Associate*, vol.46, pp.68-78, 1951. [online], available: http://www.jstor.org/stable/2280095

[8] A. Abdi and M. Kaveh, "K distribution: an appropriate substitute for Rayleigh-lognormal distribution in fading shadowing wireless channels," *Electron. Lett.*, vol.34, pp.851-852, Apr. 1998.

[9] G. Stüber, *Principles of Mobile Communication*, second edition, Kluwer Academic, 2000. Chapter 2.

[10] D. A. Abraham and A. P. Lyons, "Novel physical interpretations of K-distributed reverberation," *IEEE J. Ocean. Eng.*, vol.27, pp.800-813, Oct. 2002.

[11] P. A. van Walree, T. Jenserud and M. Smedsrud, "A discrete-time channel simulator driven by measured scattering functions," *IEEE J. Sel. Areas in Commun.*, vol.26, pp.1628-1637, Dec. 2008.

[12] T. S. Rappaport, *Wireless Coomunications: Principle and Practice*, second edition, Prentice Hall, 2002.

2. Statistical Channel Modeling of Wireless Shallow Water Acoustic Communications from Experiment Data

Jian Zhang, Jesse Cross, and Yahong Rosa Zheng
Department of Electrical and Computer Engineering,
Missouri University of Science and Technology, Rolla, MO, 65409, USA

Abstract

This paper analyzes statistical characteristics of underwater acoustic channels estimated by ocean experimental data. The baseband complex channel impulse responses (CIRs) are estimated by a time-domain least square method with sliding windows applied to long probing sequences. The probability density functions (PDF) of the real part, imaginary part, magnitude, and phase of the CIR are evaluated, and the two-sample Kolmogorov-Smirnov test is used to measure fitness of the magnitude PDF to the Gamma, Rayleigh, and compound-K distributions. The second-order statistics of the channel are also investigated in terms of autocorrelation function, channel coherence time, and scattering function. The experimental results demonstrate that underwater channels are often worse than Rayleigh fading channels.

2.1. Introduction

Underwater acoustic (UWA) propagation is proven to be the effective means of underwater wireless communication for medium and long ranges (1 km – 1000 km). However, underwater acoustic channels, especially shallow water horizontal channels, are often more challenging than radio frequency (RF) channels due to excessive path loss, complicated propagation mechanism, and time-varying inhomogeneous media. Statistical modeling of RF channels has been well established in the literature and has played important roles in capacity analysis, transceiver design, and performance evaluation.

However, analysis and modeling of UWA channels focused on the acoustic wave propagation mechanism in the past and limited studies are available for extracting statistical properties [1, 2].

Extensive ocean experiments have been conducted over the past two decades and existing UWA channel statistics studies show that UWA channels are often worse than Rayleigh fading, which in turn heavily impacts the bit error rate (BER) performance [4,4]. Multipath and Doppler effect of UWA are described in [1, 2] providing guidelines in equalizer design. Wideband UWA channel is modeled in [5] recently. It is shown that UWA channel capacity is also greatly impacted by accurate channel models [6].

This paper analyzes ocean experiment data collected in the Reschedule Acoustic Communication Experiment (RACE), Narragansett Bay, Rhode Island, March 2008, and investigates the statistical characteristics of UWA channels, including the probability density function (PDF), autocorrelation function, crosscorrelation function, and scattering function of the baseband equivalent channel impulse responses (CIRs). The complex CIRs are estimated by a sliding window least square method, where small window length and sliding width are used for long probing data sequences to accurately track the time-varying CIRs. The Kolmogorov-Smirnov (KS) test [7] is employed to statistically test the fitness between the PDF of estimated CIRs and theoretical PDFs. The test results show that the experimental channel magnitude PDF matches the compound K distribution with small shape parameters. Our results also show that the phases of CIRs are approximately uniform in $[0, 2\pi]$ and the autocorrelation function exhibits exponential decay that is dominated by the Gamma component of the compound-K distribution. The channel scattering function is obtained from the correlation function providing channel characteristics in the delay-doppler plane.

2.2. Channel model and channel statistics

Let $\tilde{s}(t)$ denote the baseband equivalent complex signal and $S(t) = \mathrm{Re}\{\tilde{s}(t)e^{j2\pi f_c t}\}$ denote the passband transmit signal with a carrier frequency f_c. At the receiver, the

received signal is $R(t) = \mathrm{Re}\{\tilde{r}(t)e^{j2\pi f_c t}\}$, where $\tilde{r}(t)$ is baseband complex envelop. Then $\tilde{r}(t)$ can be represented as

$$\tilde{r}(t) = \int h(t,\tau)\tilde{s}(t-\tau)d\tau \tag{2.1}$$

where $h(t,\tau)$ is the equivalent complex baseband impulse response for a time-varying frequency-selective channel. In a multipath and Doppler spread propagation environment, we assume there are I multi-paths and each path has distinguished delay and Doppler shift. Then, the channel impulse response is modeled as

$$h(t,\tau) = \sum_{i=1}^{I} A_i \cdot e^{j2\pi(f_{d,i}t - f_{d,i}\tau_i - f_c\tau_i)} \cdot \delta(\tau - \tau_i) \tag{2.2}$$

where A_i, τ_i, and $f_{d,i}$ are the gain, propagation delay, and instantaneous Doppler shift at the i-th path. Although the time-varying channel results in time-varying A_i, τ_i, and $f_{d,i}$, these parameters can be assumed to be constant in a short time interval, which is the so called quasi-static channel.

2.2.1. Channel Estimation. A time-domain least squares (LS) method is employed in this paper to probe the channel impulse response (CIR) from the baseband input and output signals. A long probing sequence is transmitted by the transducer and the CIRs are estimated progressively by using a sliding window of size N_p.

Let $\mathbf{s}_n^p$ denote the probing symbols of the n-th transducer at the p-th step. The estimated time-domain CIR for the m-th hydrophone is $\hat{\mathbf{h}}_m^p = [(\hat{\mathbf{h}}_{m,1}^p)^T, \cdots, (\hat{\mathbf{h}}_{m,N_t}^p)^T]^T$, where $\hat{\mathbf{h}}_{m,n} = [\hat{h}_{m,n}^s(1), \cdots, \hat{h}_{m,n}^s(L)]^T$ with a channel length L and N_t is the number of transducers, can be estimated as

$$\hat{\mathbf{h}}_m^p = (\mathbf{s}^p)^\dagger \cdot \mathbf{r}_m^p \tag{2.3}$$

where $()^{\dagger}$ denotes the pseudo inverse, $\mathbf{r}_m^p = [r_m^p(L), \cdots, r_m^p(N_p)]^T$ which is the corresponding MIMO channel output vector, and $\mathbf{s}^p = [\mathbf{T}_1^p | \cdots | \mathbf{T}_{N_t}^p]$ with

$$\mathbf{T}_n^p = \begin{bmatrix} s_n^p(L) & s_n^p(L-1) & \cdots & s_n^p(1) \\ s_n^p(L+1) & s_n^p(L) & \cdots & s_n^p(2) \\ \vdots & \ddots & \ddots & \vdots \\ s_n^p(N_p) & s_n^p(N_p-1) & \cdots & s_n^p(N_p-L+1) \end{bmatrix} \tag{2.4}$$

where $n = 1, \cdots, N_t$. Let N_d denote the sliding step of the data window. The CIR is re-estimated every $N_d T_s$ interval, where T_s is the symbol period.

2.2.2. Magnitude Distributions. Let X have a Rayleigh distribution with a parameter σ, then the conditional PDF of X is given as

$$f_X(x) = \frac{x}{\sigma^2} \exp(-\frac{x^2}{2\sigma^2}) \tag{2.5}$$

The PDF of a Gamma distributed X is given as

$$f_X(x) = \frac{1}{b^a \Gamma(a)} x^{a-1} \exp(-\frac{x}{b}) \tag{2.6}$$

where $\Gamma(\cdot)$ is the Euler gamma function and a and b are scalar parameters.

The unconditioned PDF of X, if X has a compound K distribution, is given as

$$f_X(x) = \frac{4}{\sqrt{\beta}\Gamma(\nu)} \Big(\frac{x}{\sqrt{\beta}}\Big)^{\nu} K_{\nu-1}\Big(\frac{2x}{\sqrt{\beta}}\Big) \tag{2.7}$$

where $K_{\nu-1}$ is the modified bessel function of the second kind of order $\nu - 1$. A Rayleigh distribution results when $v \to \infty$ and $\beta\nu = 2\sigma^2$ remains constant. Therefore, as ν decreases the channel gets worse than Rayleigh fading.

The first and second moments were used to fit the PDFs of the different distributions to the measured data and are given in the Table 2.1.

Table 2.1 The first and second moments of Rayleigh, Gamma, and Compound k Distributions

	Rayleigh	Gamma	Compound K
$E(x)$	$\sigma\sqrt{(\frac{\pi}{2})}$	ab	$\frac{\sqrt{\beta\pi}}{2} \cdot \frac{\Gamma(\nu+0.5)}{\Gamma(\nu)}$
$E(x^2)$	$\frac{4-\pi}{2}\sigma^2$	ab^2	$\beta\nu$

2.2.3. Kolmogorov-Smirnov (KS) Test. The KS test is one of the most useful and general nonparametric tools to quantify the similarity of two empirical distribution functions. The two-sample KS test can serve as a goodness of fit test, and is used to determine if two datasets share a common probability distribution. No assumptions are made about the distributions of the two datasets. The null hypothesis of the KS test is that both datasets do not differ significantly and therefore follow the same distribution. The alternative hypothesis is that the two datasets follow different distributions. The Kolmogorov-Smirnov statistic D is defined as

$$D_{n,n'} = \sup_x |F_n(x) - F_{n'}(x)| \tag{2.8}$$

where $F_n(x)$ and $F_{n'}(x)$ are the empirical cumulative distribution functions (CDF) of the two distributions to be compared and sup is the supremum of the set $|F_n(x) - F_{n'}(x)|$.

The alternative hypothesis will be accepted at level α if

$$Q_\alpha < D_{n,n'}\sqrt{\frac{nn'}{n+n'}} \tag{2.9}$$

where Q_α is found by $P(Q \leq Q_\alpha) = 1 - \alpha$ and Q is a Kolmogorov distributed random variable; n and n' are the number of samples in the compared distributions, respectively.

2.2.4. Channel Scattering Function. Generally, the channel impulse response $h(t, \tau)$ is considered as a two-dimensional random process for frequency selective channels.

The general second-order autocorrelation function of $h(t,\tau)$ can be written as

$$R_h(t_1,t_2;\tau_1,\tau_2) = \mathrm{E}[h(t_1,\tau_1)h^*(t_2,\tau_2)]. \tag{2.10}$$

To simplify this four-dimensional correlation function, we make an assumption that the channel is wide sense stationary in the short term, *i.e*, the second-order statistics depends only on the difference between time instants, rather than the absolute time. Therefore, the autocorrelation of $h(t,\tau)$ is simplified as

$$\mathrm{E}(h(t+\Delta t,\tau_1)\cdot h^*(t,\tau_2)) = R_h(\Delta t,\tau_1)\delta(\tau_1-\tau_2) \tag{2.11}$$

and the channel scattering function is defined by [11]

$$S(f,\tau) = \int_{-\infty}^{\infty} R_h(\Delta t,\tau)e^{-j2\pi f\Delta t}d\Delta t \tag{2.12}$$

The two-dimensional scattering function (2.12) depicts the power spectral density of the channels along the geotime and completely describes the second-order statistics of a stationary fading channel.

2.3. Experimental results

The underwater experiment, named as Reschedule Acoustic Communication Experiment (RACE), was conducted in Narragansett Bay, Rhode Island, by Woods Hole Oceanographic Institution (WHOI), in March 2008. The water depth varied between 9 to 14 meters. The transmitter with an array of two transducers was fixed on a tripod and was four meters above the sea bottom. The receiver with an array of 12 hydrophones was also fixed on a tripod and was located two meters above the sea bottom. In this study, the data was collected when the distance between the transmitter and receiver was 1000 meters. The carrier frequency was $f_c = 11.5$ kHz, the sampling rate $f_s = 39.0625$ kHz, and the bandwidth $B = f_s/10 = 3.90625$ kHz.

A probing sequence with a duration of 22 seconds was transmitted to probe the channel impulse responses. A sliding window was used with a window size $N_p = 128$ and the interval between adjacent window $N_d = 32$. Hence, the sampling rate at the absolute time domain is $1/(32 \cdot T_s) = 122$ Hz which means the channels are estimated in every 8.2 milliseconds. The channel impulse responses (CIRs) were estimated progressively by the LS method described in (2.3). For each tap, 2144 samples were obtained in one probing data packet. The two-dimensional time-varying CIRs for the subchannel corresponding to (Tx1, Rx1) and (Tx2, Rx1) are plotted in Fig. 2.1(a) and Fig. 2.1(b). The frequency-selective channel length spans 25 symbol periods.

Fig. 2.2(a) and Fig. 2.2(b) show the real and imaginary parts of the measured data distribution versus a Gaussian distribution with the same mean and different variances. We can see the measured PDFs of the real and imaginary parts do not follow the Gaussian distribution. For the probability densities around large values, the Gaussian distribution with large variance matchs the tails of the measured PDFs. However, for the probability densities at small values, the Gaussian distributions with small variance fit the peaks of the measured PDFs better.

Since the real and imaginary parts are not well represented by Gaussian distributions, it is reasonable to predict the magnitude probability distribution will not follow a Rayleigh distribution. Fig. 2.2(c) shows the measured magnitude PDF versus fitted compound K and other distributions. It can be seen visually that the Rayleigh and Gamma distributions are not a good fit. The KS test was used to compare the measured PDF with different distributions to find the best match to the measured PDF. The KS test results for different distributions are depicted in Table 2.2. In this table, the p-value is associated with a test statistic, which represents the probability of a test statistic at extreme as the one actually observed. If the significance level $\alpha = 5\%$, the null hypothesis is rejected when the p-value is less than 0.05. The $D_{n,n'}$ is the maximum distance between two CDFs, and the results has two choice: reject or accept the null hypothesis. The fittest parameters for different distributions were chosen from the KS

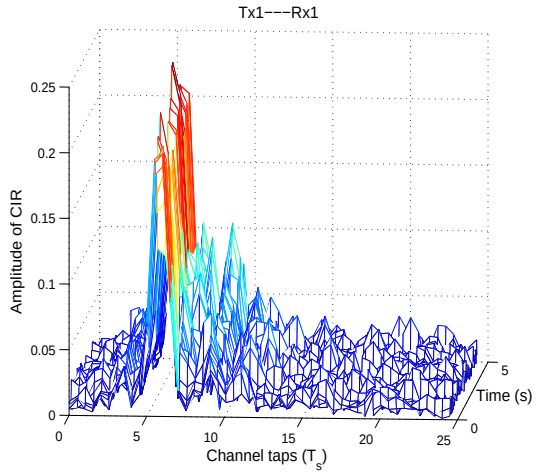

(a) Estimated CIRs for the subchannel Tx1—Rx1

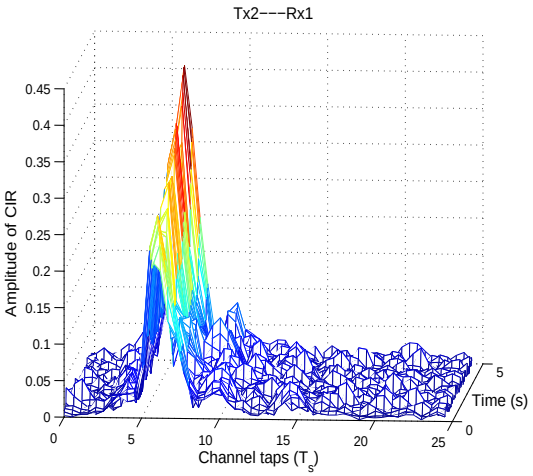

(b) Estimated CIRs for the subchannel Tx2—Rx1

Figure 2.1 Estimated time-varying frequency-selective channel impulse responses.

test that returned the highest p-value. The null hypothesis which asserts the measured distribution follows the fitted compound K distribution with $\nu = 0.63$ and $\beta = 6.04$ was accepted with a p-value of 0.96 and $D_{n,n'} = 0.07$. However, the null hypothesis when the measured data is subject to the best fit Rayleigh distribution is rejected with a very small p-value, 1.1×10^{-51}. The null hypothesis when compared to the fitted Gamma distribution is rejected with a p-value of 1.18×10^{-6}. Therefore, we conclude that the measured data follows a compound K distribution rather than a Rayleigh or Gamma distribution.

Table 2.2 The Kolmogorov-Smirnov results for the measured PDF when compared to different fitted distributions

	Gamma	Rayleigh	Compound K
p-value	1.18×10^{-6}	1.1×10^{-51}	0.96
$D_{n,n'}$	0.16	0.48	0.07
Results	reject	reject	accept

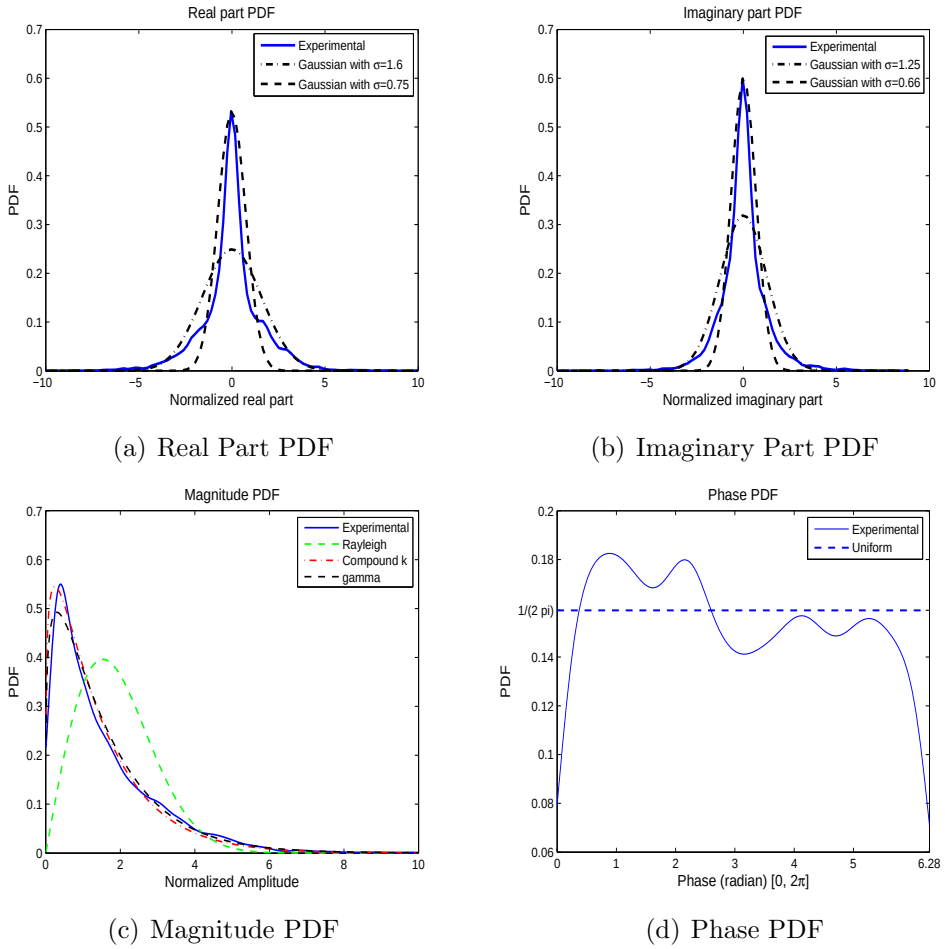

(a) Real Part PDF

(b) Imaginary Part PDF

(c) Magnitude PDF

(d) Phase PDF

Figure 2.2 The PDFs of the complex CIR. (a) PDF of real part versus Gaussian with $\sigma = 1.6$ and 0.75. (b) PDF of imaginary part versus Gaussian with $\sigma = 1.25$ and 0.66. (c) PDF of magnitude versus compound K and other distributions. (d) PDF of phase versus uniform distribution.

The normalized autocorrelation functions of each channel tap for real part, imaginary part and complex envelop are depicted in Fig. 2.3. It is noted that these three

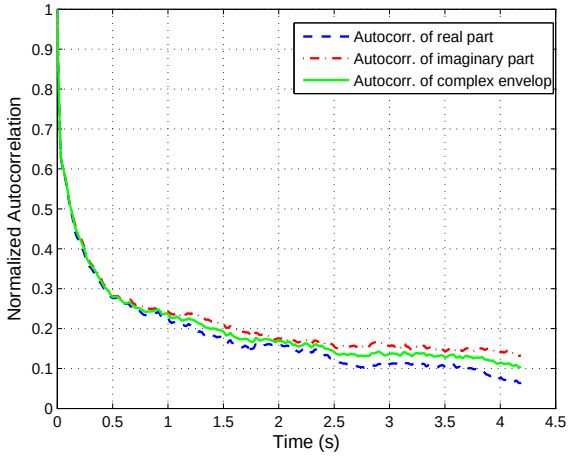

Figure 2.3 The normalized autocorrelation of the real part, imaginary part, and complex envelop of the CIR. The autocorrelation function is dominated by the Gamma component of the CIR.

autocorrelation curves behave similarly all with exponential decay. Define the channel coherence time as the time over which the autocorrelation is above 0.5. The coherence time was approximately $T_c = 0.12s$ for this channel. It implies that the channel can be considered to be invariant if the length of data block is less than $T_c \cdot B \approx 470$ symbols. The relation between the coherence time and the maximum Doppler spread is given by [12]

$$T_c \approx \frac{9}{16\pi f_m} \tag{2.13}$$

where f_m is maximum Doppler shift. In this case, $f_m = 1.5$ Hz and the dynamic range of the instantaneous Doppler spread is $[-1.5, 1.5]$ Hz. Figure 2.4 shows the cross correlation of the real and imaginary part of the CIR. It is seen that the real parts and the imaginary part are uncorrelated.

The two-dimensional scattering function is shown in Fig. 2.5 by performing Fourier transform on the correlation function. We see that the average Doppler shift is very small, close to zero Hz since the transceiver platforms were always fixed during the experiment and the motion of the wave was not significant. From the power spectral density, the channel has a Doppler spread of $[-1.5, 1.5]$ Hz at a delay of $1 \sim 2.5$ ms.

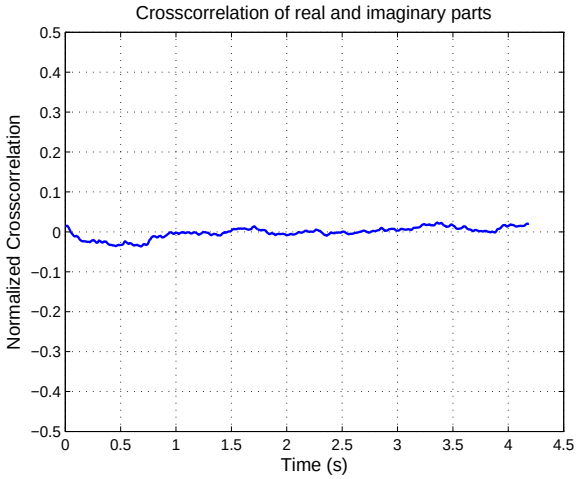

Figure 2.4 The normalized cross correlation between the real and imaginary parts of the CIR. The real and imaginary parts are uncorrelated.

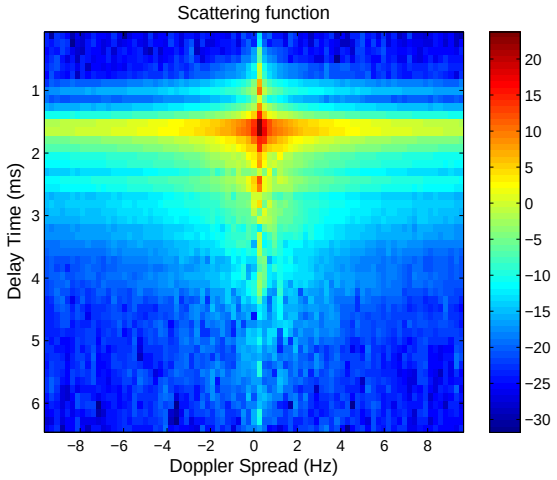

Figure 2.5 The channel scattering function

2.4. Conclusion

In this paper, we presented the statistical characteristics, including PDF and second-order statistics, for the UWA channels measured in RACE, 2008. Experimental results

demonstrate that the real and imaginary parts of the complex UWA channels do not follow Gaussian; the PDF of the magnitude fits the compound K distribution; the PDF of phase approximately follows uniform distribution. The autocorrelations of CIRs behave like decaying exponential curves and the channel coherence time is also roughly estimated. The scattering function provides better understanding on the spectral density of the UWA channels.

2.5. Acknowledgment

This work was supported in part by the National Science Foundation under Grant ECCS-0846486 and the Office of Naval Research under Grants N00014-10-1-0174. The authors are grateful to Dr. J. Preisig for his leadership of conducting the RACE08 experiments.

References

[1] M. Stojanovic and J. Preisig, "Underwater acoustic communication channels: propagation models and statistical characterization," *IEEE Commun. Mag.*, pp.84-89, Jan. 2009.

[2] A. C. Singer, J. K. Nelson, S. S. Kozat, "Signal processing for underwater acoustic communications," *IEEE Commun. Mag.*, pp.90-96, 2009.

[3] W. Yang and T. C. Yang, "High frequency channel characterization for M-ary frequency-shift keying underwater acoustic communications," *J. Acoust. Soc. Am.*, vol.120, pp.2615-2626, Nov. 2006.

[4] W. Yang and T. C. Yang, "M-ary frequency shift keying communications over an underwater acoustic channel: performance comparison of data with models," *J. Acoust. Soc. Am.*, vol.120, pp.2694-2701, Nov. 2006.

[5] A. G. Zajić, "Statistical space-time-frequency characterization of MIMO shallow water acoustic channels," in *Proc. IEEE OCEANS'09*, Bloxi, MS, USA, Oct. 26-29, 2009.

[6] T. J. Hayward and T. C. Yang, "Single-and multi-channel underwater acoustic communication channel capacity: A computational study," *J. Acoust. Soc. Am.*, vol.22, pp.1652-1661, Sep. 2007.

[7] F. J. Massey, "The Kolmogorov-Smirnov test for goodness of fit," *J. Am. Stat. Associate*, vol.46, pp.68-78, 1951.

[8] A. Abdi and M. Kaveh, "K distribution: an appropriate substitute for Rayleigh-lognormal distribution in fading shadowing wireless channels," *Electron. Lett.*, vol.34, pp.851-852, Apr. 1998.

[9] G. Stüber, *Principles of Mobile Communication*, second edition, Kluwer Academic, 2000.

[10] D. A. Abraham and A. P. Lyons, "Novel physical interpretations of K-distributed reverberation," *IEEE J. Ocean. Eng.*, vol.27, pp.800-813, Oct. 2002.

[11] P. A. van Walree, T. Jenserud and M. Smedsrud, "A discrete-time channel simulator driven by measured scattering functions," *IEEE J. Sel. Areas in Commun.*, vol.26, pp.1628-1637, Dec. 2008.

[12] T. S. Rappaport, *Wireless Coomunications: Principle and Practice*, second edition, Prentice Hall, 2002.

3. Impact of Spatial Correlation of Fading Channels on the Performance of MIMO Underwater Communication Systems

Jesse Cross, Jian Zhang, and Yahong Rosa Zheng
Department of Electrical and Computer Engineering,
Missouri University of Science and Technology, Rolla, MO, 65409, USA

Abstract

The spatial and intertap correlation matrices of fading channels is first estimated for underwater multiple input multiple output (MIMO) systems using real experimental data. We confirm that underwater MIMO channels exhibit strong spatial and temporal correlation. The bit error rate (BER) performance of the MIMO system at different correlation scenarios are also evaluated with computer simulation. At BER=0.01%, the required SNR of highly correlated channel is 5 dB higher than the i.i.d. channel. BER results of the experimental data also quantitatively show the performance degradation caused by the correlation.

3.1. Introduction

Underwater acoustic (UWA) transmission is an effective method used for communication over medium and long ranges (1-1000 km); however, many aspects of UWA channels present additional challenges when compared to in air radio frequency (RF) channels. UWA channels exhibit time variance, large multipath delay times, frequency dependent fading, and slow wave propagation speed. The time variance is caused by changes in the environment such as changes in the speed of the transmitters, receivers, or the media,itself, and turbulence caused by surface waves and vehicles. Additional computational complexity results when the channel must be re-estimated, repeatedly. The multipath delay times may be on the order of tens to hundreds of milliseconds resulting in great intersymbol interference (ISI) and channel impulse responses (CIR) that have many more taps than an RF CIR. The frequency dependent fading severely limits the

bandwidth available for data transmission. Waves that propagate more slowly are more affected by small Doppler shifts and spread.

Data collected in the Surface Process and Acoustic Communications Experiment conducted in fall 2008 (SPACE08) by the Woods Hole Oceanographic Institute (WHOI) is investigated. The effects of spatial correlation on the BER are investigated. It is shown that the a smaller amount of receivers may be used in place of a larger number of receivers with a very small impact on the BER as long as the aperture is the same. The Kronecker properties of the spatial correlation matrix are analyzed. The matrix is decomposed into a series of Kronecker products and the error resultant matrix formed by the decomposed matrices and the original matrices is quantified. A simulation is conducted to confirm the experimental results are due to spatial correlation.

3.2. MIMO Acoustic Communication Systems

The system may be generalized as a MIMO system with P transmitters and Q receivers. The baseband equivalent discrete time domain signal at the q_{th} receiver is defined as

$$y_q(k) = \sum_{p=1}^{P} \sum_{l=1}^{L} h_{q,p}(l,k) x_p(k+1-l) + w_q(k) \tag{3.1}$$

where L is the channel length; $h_{q,p}(l,k)$ is the l_{th} CIR coefficient at time, k; T is the symbol interval; $f_{q,p,k}$ is the instantaneous Doppler shift between transmitter, p, and receiver, q; $\theta_{q,p}$ is the initial phase error present in the q,p subchannel; and $w_q(k)$ is zero mean white Gaussian noise with variance, σ_w^2, present at receiver, q.

The complete MIMO system is modeled in matrix form as

$$\begin{aligned} \mathbf{y} &= \begin{bmatrix} \mathbf{h}_{1,1} & \cdots & \mathbf{h}_{1,P} \\ \vdots & \ddots & \vdots \\ \mathbf{h}_{Q,1} & \cdots & \mathbf{h}_{Q,P} \end{bmatrix} \begin{bmatrix} \mathbf{x}_1 \\ \vdots \\ \mathbf{x}_P \end{bmatrix} + \begin{bmatrix} \mathbf{w}_1 \\ \vdots \\ \mathbf{w}_Q \end{bmatrix} \\ &= \mathbf{H} \cdot \mathbf{x} + \mathbf{w} \end{aligned} \tag{3.2}$$

where the received vector is $\mathbf{y} = [\mathbf{y}_1^T, \cdots, \mathbf{y}_Q^T]^T$. The signal received at each hydrophone may be represented as $\mathbf{y}_q = [y_q(1), \cdots, y_q(N)]^T$. $\mathbf{x}_p = [x_p(1), \cdots, x_p(N)]^T$ is the signal transmitted by the p_{th} transducer where $x_p([N_d + 1, \cdots, N]) = 0$.
$\mathbf{D}_{q,p} = \text{diag}\{e^{j(2\pi T f_{q,p,1} + \theta_{q,p})}, \cdots, e^{j(2\pi N T f_{q,p,N} + \theta_{q,p})}\}$. $\mathbf{h}_{q,p}$ is the $(p,q)_{th}$ CIR with the diagonal phase components missing.

It is assumed the coherence time of the channel is greater than the block duration which implies the channel may be considered time invariant over one block.

3.2.1. Channel Estimation.

A time domain least squares method is used to estimate the channel from the data contained in the transmitted blocks. The transmitted data matrix at the p_{th} transmitter, $\mathbf{x}_{td}$, is defined as

$$\mathbf{x}_{td} = \begin{bmatrix} x_{td}(L) & x_{td}(L-1) & \cdots & x_{td}(1) \\ x_{td}(L+1) & x_{td}(L) & \cdots & x_{td}(2) \\ \vdots & \ddots & \ddots & \vdots \\ x_{td}(N_d) & x_{td}(N_d - 1) & \cdots & x_{td}(N_d - L + 1) \end{bmatrix} \tag{3.3}$$

where N_d is the number of data symbols used in the estimation.

The subchannel impulses involving receiver, q, are defined as $\hat{\mathbf{h}}_q = [\lambda_{q,1}\hat{\mathbf{h}}_{q,1}^T, \cdots, \lambda_{q,P}\hat{\mathbf{h}}_{q,P}^T]^T$. The estimation is performed using (3.4).

$$\hat{\mathbf{h}}_q = \mathbf{x}_t^\dagger \cdot \mathbf{y}_{tq} \tag{3.4}$$

where $\mathbf{x}_t = \left[\mathbf{x}_{t1}, \ \cdots, \ \mathbf{x}_t\right]$, $(\cdot)^\dagger$ denotes the pseudo-inverse, and $\mathbf{y}_{tq} = [y_{tq}(L), \cdots, y_{tq}(N_P)]^T$ denotes the received data symbols at hydrophone, q.

3.2.2. Frequency Domain Turbo Equalization.

The incoming data blocks are converted to the frequency domain with a simple FFT. The vector $\mathbf{Y}_p$ is the frequency domain representation on the incoming data. The

MMSE FDTE adaptively computes new coefficients using the *a priori* mean and variance of the incoming data in order to estimate the symbols sent.

8PSK was used as the modulation technique of all estimations. The symbol alphabet used is $\mathcal{S} = [1, \frac{1}{\sqrt{2}}(1+j), j, \frac{1}{\sqrt{2}}(-1+j), -1, \frac{1}{\sqrt{2}}(-1-j), -j, \frac{1}{\sqrt{2}}(1-j)]$ for the bit patterns, $[d_{m,1}d_{m,2}d_{m,3}] \in \{111, 110, 010, 000, 100, 101, 001, 011\}$, respectively. The mean, $\mu_{p,k}$, and variance, $\nu_{p,k}$, are calculate using

$$\begin{aligned} \mu_{p,k} &= 1/4 \cdot \big((l_1 - 1) \cdot (l_3 + l_2) - \sqrt{2} \cdot (l_2 + l_1 \cdot l_3)\big) \\ &\quad + j \cdot 1/4 \cdot \big((l_1 + 1) \cdot (l_3 - l_2) + \sqrt{2} \cdot (l_3 + l_1 \cdot l_2)\big) \\ \nu_{p,k} &= 1 - |\mu_{p,k}|^2 \end{aligned} \tag{3.5}$$

where $l_g = \tanh\big(L_a^D(c_{p,3(k-1)+g})/2\big)$. $c_{p,k}$ is the coded bit and $L_a^D(\cdot)$ is the *a priori* log likelihood ratio of the decoded bit.

The MMSE equalized symbols are represented in the frequency domain as

$$\hat{\mathbf{X}}_p(k) = K_p^{-1} \cdot \mathbf{U}_p^H \cdot (\mathbf{Y} - \hat{\mathbf{H}} \cdot \bar{\mathbf{X}} + \mu_{p,k}\hat{\mathbf{H}}\mathbf{F}_P\mathbf{u}_{p,k}) \tag{3.6}$$

where $\hat{\mathbf{H}}$ is the frequency domain channel matrix; $\mathbf{F}_P$ is the normalized DFT matrix; and $\mathbf{u}_{p,k}$ is a vector of length PN where element, $((p-1)N + k)$, is 1 and the other elements are zero. The vector $\bar{\mathbf{X}}$ is the mean of the incoming symbols in frequency domain as is defined as

$$\bar{\mathbf{X}} = \mathbf{F}_P[\bar{\mathbf{x}}_1^T, \cdots, \bar{\mathbf{x}}_P^T]^T, \tag{3.7}$$

where $\bar{\mathbf{x}}_p = [\mu_{p,1}, \cdots, \mu_{p,N}]^T$.

The equalizer coefficients, $\mathbf{U}_p$, are

$$\mathbf{U}_p = (\sigma_w^2\mathbf{I}_{QN} + \hat{\mathbf{H}} \cdot \bar{\mathbf{V}} \cdot \hat{\mathbf{H}}^H)^{-1} \cdot \hat{\mathbf{H}} \cdot \begin{bmatrix} \mathbf{O}_{(p-1)N \times N} \\ \mathbf{I}_N \\ \mathbf{O}_{(P-p)N \times N} \end{bmatrix} \tag{3.8}$$

where $\mathbf{O}_{m\times n}$ is a zero matrix and $\bar{\mathbf{V}}$ is

$$\bar{\mathbf{V}} = \text{diag}\big\{\bar{\nu}_1\mathbf{I}_N, \quad \cdots \quad, \bar{\nu}_P\mathbf{I}_N, \big\}, \tag{3.9}$$

where $\bar{\nu}_p$ is the mean of ν_p and the scalar K_p is

$$K_p = 1 + \frac{1-\bar{\nu}_p}{N}\text{Tr}\{\hat{\mathbf{H}}^H_{(\bullet,pN-N+1:pN)}\mathbf{U}_p\}, \tag{3.10}$$

where $\hat{\mathbf{H}}_{(\bullet,i:j)}$ denotes the matrix composed of the i-th to j-th columns of $\hat{\mathbf{H}}$.

The time domain symbols for the transmitter in (3.6) are

$$\hat{x}_p(k) = \mathbf{F}^H_{(\bullet,\ k)} \cdot \hat{\mathbf{X}}_p(k), \tag{3.11}$$

where $\mathbf{F}_{(\bullet,\ k)}$ represents column, k of the DFT matrix $\mathbf{F}$.

3.2.3. Spatial Correlation.

A MIMO system may be modeled as $\mathbf{Y} = \mathbf{HX} + \mathbf{W}$ where channel matrix, $\mathbf{H}$, is defined by

$$\mathbf{H} = \begin{bmatrix} \mathbf{h}_{1,1} & \cdots & \mathbf{h}_{1,P} \\ \vdots & \ddots & \vdots \\ \mathbf{h}_{Q,1} & \cdots & \mathbf{h}_{Q,P} \end{bmatrix} \tag{3.12}$$

In [1], the spatial correlation is defined as the Kronecker product of the transmitter, receiver, and intertap correlation matrices. The spatial correlation between receivers q_1 and q_2 is defined as

$$\mathbf{R}_{q_1q_2} = E\{h_{vec}h^T_{vec}\} = \Psi_{Tx} \otimes \Psi_{Rx} \otimes \Psi_{tap} \tag{3.13}$$

where in a two transmitter MIMO system, $h_{vec} = [h_{q_1p_1}, h_{q_1p_2}, h_{q_2p_1}, h_{q_2p_2}]$. The Kronecker product is represented by $\otimes$. Matrices Ψ_{Tx}, Ψ_{Rx}, and Ψ_{tap}, are the transmitter, receiver, and intertap correlation matrices, respectively.

The transmitter correlation matrix may be factored out by using

$$\begin{aligned}\mathbf{R}_{q_1q_2} &= E\{h_{Rx}h_{Rx}^T\} = \Psi_{Rx} \otimes \Psi_{tap} \\ &= \begin{bmatrix} \Psi_{q_1q_1}\Psi_{tap} & \Psi_{q_1q_2}\Psi_{tap} \\ \Psi_{q_2q_1}\Psi_{tap} & \Psi_{q_2q_2}\Psi_{tap} \end{bmatrix}\end{aligned} \tag{3.14}$$

where $h_{Rx} = [h_{q_1p_1}, h_{q_2p_1}]$.

A metric that may be used to quantify the similarity of two correlation matrices was described in [2]. The correlation matrix distance (CMD) is defined as

$$d_{corr}(\mathbf{R}_1, \mathbf{R}_2) = 1 - \frac{tr\{\mathbf{R}_1\mathbf{R}_2\}}{||\mathbf{R}_1||_f||\mathbf{R}_2||_f} \quad \in [0, 1] \tag{3.15}$$

where $tr\{\cdot\}$ is the trace operator and $||\cdot||_f$ is the Frobenius norm. The CMD will return as zero for matrices that are identical save for a scaling factor and one for matrices that are maximally distant.

The CMD is based upon the inner product and measures the angle between the two correlation matrices in $n \times n$ dimensional space. Matrices that are identical up to a scaling factor have no angle between them so the CMD will return $1 - cos(0) = 0$.

The CMD is useful when comparing a measured correlation matrix to an estimated correlation matrix because it gives a quantifiable method to determine the difference between the spatial structure (and therefore channel characteristics) of the measured and estimated channels.

3.3. Experiment Results

This paper analyzes channel spatial correlation through data collected in the Surface Process and Acoustic Communications Experiment conducted in fall 2008 (SPACE08) by the Woods Hole Oceanographic Institute (WHOI). The experiment took place in shallow water (about 15 meters deep) south of Cape Cod, MA. The distances between the transmitter array and receiver array were 200 m and 1000 m. The transmitters were

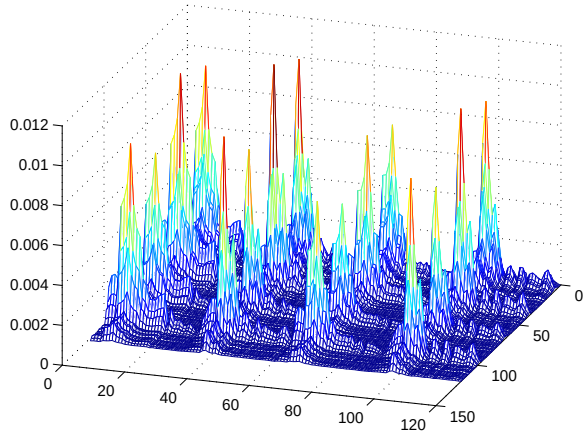

Figure 3.1 Magnitude of the channel correlation matrix of a 2x2 MIMO channel

fixed on a tripod with the top transmitter 3 m above the sea floor with 50 cm spacing between the transmitters. The receivers were also fixed upon a tripod. At 200 m, there were 24 receivers with a spacing of 5 cm. At 1000 m, there were 12 receivers with a spacing of 12 cm. The carrier frequency was 13 kHz; the sampling frequency, F_s, was 39.0625 kHz; and the bandwidth was $F_b = F_s/4 = 9.7656$ kHz.

3.3.1. Spatial Correlation.

Measurements taken during the experiment show a decrease in spatial correlation as the receivers are spaced further apart. Figure 3.1 shows the spatial correlation matrix between receivers one and two. The correlation matrices between other receivers look similar. The shape of the matrix strongly suggests the Kronecker based model in [1] is applicable.

The decrease in spatial correlation may be observed when using (3.14) to factor out the transmitter correlation. Figure 3.2 shows the spatial correlation between receivers 1 and 2, 1 and 4, and 1 and 10. This figure shows the maximum and minimum spatial correlation present in the different receiver combinations analyzed above. It is evident that the spatial correlation decreases with distance.

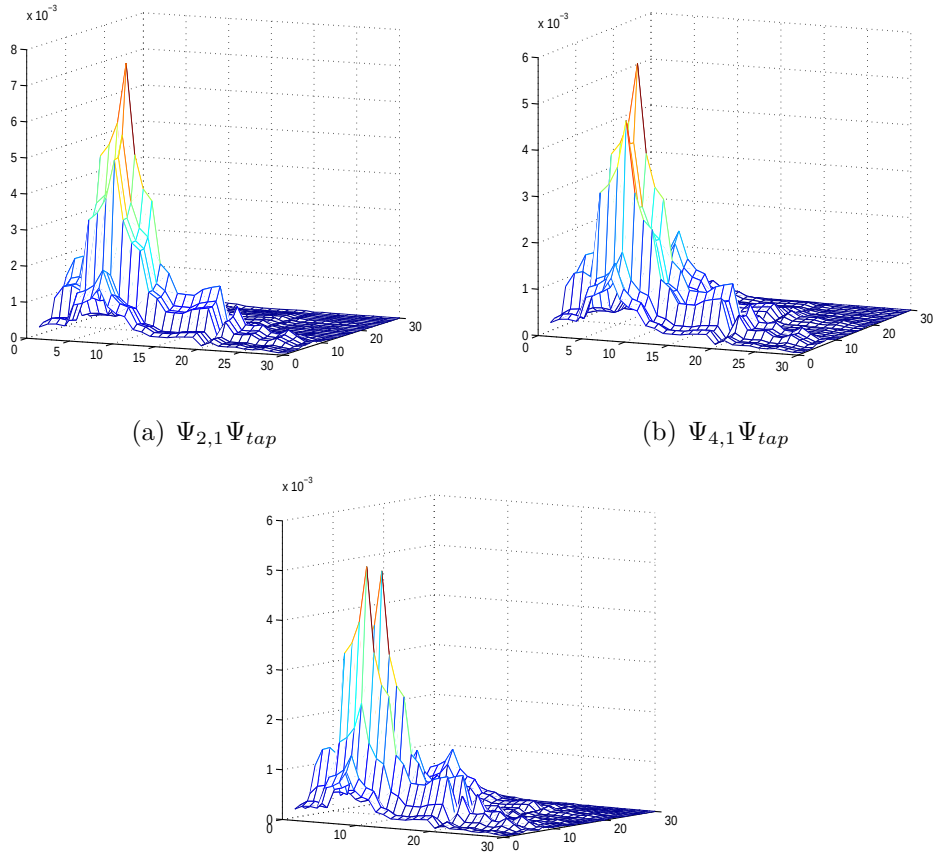

(a) $\Psi_{2,1}\Psi_{tap}$ (b) $\Psi_{4,1}\Psi_{tap}$

(c) $\Psi_{10,1}\Psi_{tap}$

Figure 3.2 Spatial correlations between different receivers

Equation (3.14) may be used to factor Ψ_{tx} out of (3.13). By using the definition of the Kronecker product in reverse and normalizing the correlations matrix in respect to the highest peak in the overall correlation matrix, the transmitter and receiver correlation matrices may be may be factored out. Representative transmitter and receiver matrices for the spatial correlation between different receivers are shown in Fig. 3.1.

The CMD calculated using the estimated matrices in Fable 3.1 and (3.15) are 0.24, .17, and .25, respectively. It is evident from these correlation matrices that the spatial correlation is decreasing as the receivers move further apart.

Table 3.1 Ψ_{Tx} and Ψ_{Rx} for hydrophones at 200 m

H_1 and H_2	$\Psi_{tx} = \begin{bmatrix} 1.0000 + j0.0000 & 0.8861 - j0.1140 \\ 0.8861 + j0.1140 & 0.7983 + j0.0000 \end{bmatrix}$ $\Psi_{rx} = \begin{bmatrix} 0.7606 + j0.0000 & 0.7692 + j0.4101 \\ 0.7692 - j0.4947 & 1.0000 + j0.0000 \end{bmatrix}$
H_1 and H_4	$\Psi_{tx} = \begin{bmatrix} 1.0000 + j0.0000 & 0.8954 - j0.2687 \\ 0.8954 + j0.2687 & 0.8741 + j0.0000 \end{bmatrix}$ $\Psi_{rx} = \begin{bmatrix} 0.6090 + j0.0000 & 0.7158 + j0.3098 \\ 0.7158 - j0.3098 & 1.0000 + j0.0000 \end{bmatrix}$
H_1 and H_{10}	$\Psi_{tx} = \begin{bmatrix} 0.8551 + j0.0000 & 0.7077 - j0.5951 \\ 0.7077 + j0.5951 & 1.0000 + j0.0000 \end{bmatrix}$ $\Psi_{rx} = \begin{bmatrix} 0.4018 - j0.0000 & 0.5961 + j0.2142 \\ 0.5961 - j0.2142 & 1.0000 + j0.0000 \end{bmatrix}$

3.3.2. Transceiver BER Performance.

The BER of MIMO configurations with different receivers spaces was calculated. It was found that a larger space between the receivers had smaller spatial correlation and therefore lower BERs. The BERs of 60 runs of 200 m data and 24 runs of 1000 m data conducted during SPACE08 were calculated while using a 2 iteration turbo equalization technique. All runs analyzed used 8PSK modulation. First, the average BER was calculated for receivers 1, 2, 3, and 4. Then the average BER of receivers 1, 4, 7, and 10, was calculated. Finally the average BER using all receivers from 1 to 10 was calculated. The average BERs were calculated for 200 m and 1000 m data. The results are shown in Table 3.2.

The MIMO receiver system with receivers 1,4,7, and 10, has the same aperture as a system with receivers 1 through 10 but less receiver power power due to the smaller

Table 3.2 Transmission distance and receiver spacing BER results

	1,2,3,4	1,4,7,10	1 through 10
200 m	1.58e-1	3.03e-2	9.97e-3
1000 m	2.23e-1	9.3E-2	9.29e-2

amount of receivers. The MIMO system using receivers 1,2,3, and 4, has the same receiver power as the system using receivers 1,4,7, and 10, yet it has a smaller aperture. The results show that the aperture is more important than receiver power. The slightly smaller BER of the ten transmitter system is explained by the greater receiver power; however, the ten transmitter system is not as efficient as the system with 1,4,7, and 10, receiver spacing. At 200 m, it took six extra receivers to decrease the 1,4,7,10 BER by about 37 percent, yet merely spacing out the same number of receivers was able to decrease the 1,2,3,4 BER by about 97 percent. At 1000 m, the advantage of increased distance between receivers is more evident. The BERs between all ten receivers and the 4 spaced receivers are nearly identical.

3.4. Simulation Results

We conducted computer simulation to verify the effect of channel spatial correlation on BER performance of the FDTE receiver. In the simulation, a MIMO 2×4 UWA system was considered with 80-tap frequency-selective channels. The maximum Doppler spread was $f_d = 1$ Hz and the symbol period was $T = 0.1024\ ms$. We adopted two sparse channel Power Delay Profiles (PDP), as shown in Fig. 3.3(a), where the total average power of each profile was normalized to one. The spatial-temporally correlated fading channel waveforms were generated by the triply-selective simulation model [1] with each ray following Rayleigh distribution [7]. The overall channel distribution of 80 taps was close to the compound K distribution as indicated by recent research on UWA fading channels [4,5]. The spatial correlation was simulated via transmit and receive spatial correlation matrices, whose elements were denoted $\Psi_{tx}(p_i, p_j)$ and $\Psi_{rx}(q_i, q_j)$, respectively.

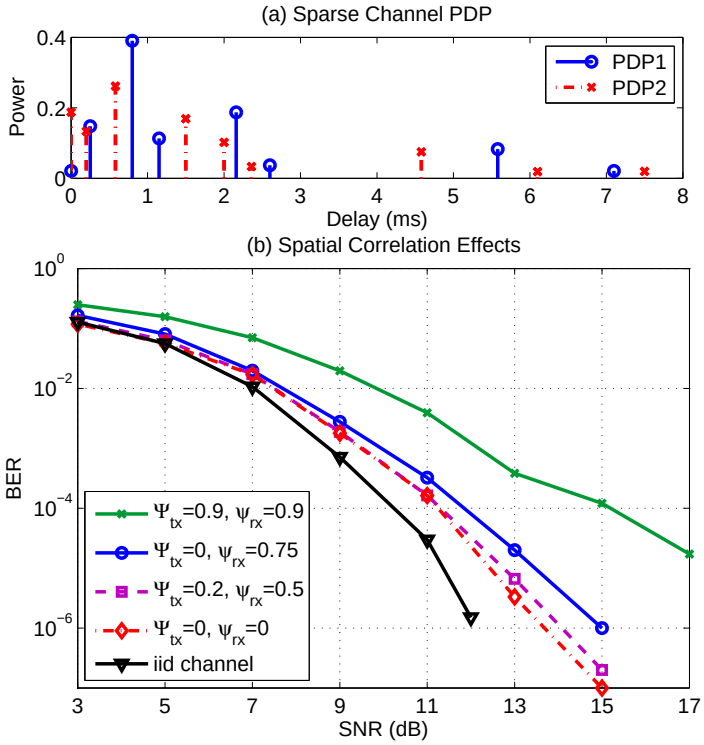

Figure 3.3 Simulation results: (a) PDP of the UWA channels with 80 taps. The normalized maximum Doppler spread was $f_d T_s = 1.024 \times 10^{-4}$. (b) BER performance of the FDTE receiver on different spatial correlations.

We selected $\Psi_{rx}(q_i, q_j) = \psi_{rx}^{|q_i - q_j|}$ to approximate the spatial correlation among the hydrophone elements since the hydrophones were equally spaced in the experiment. The encoded bits were interleaved randomly and were mapped into 8PSK symbols via Gray coding.

We applied the FDTE algorithm to recover the transmit data streams and computed the average BER via 10 to 70 trials with 76,800 information bits per trial. The BER performance in channels of different spatial correlations is depicted in Fig. 3.3(b). The BER performance in the i.i.d (independent, identically distributed) fading channels is also included in Fig. 3.3(b) as bench marks.

The spatial or intertap correlation of the MIMO channels had strong impact on the receiver performance, as illustrated in Fig. 3.3(b).The i.i.d. channel had no spatial nor intertap correlation; while the channel with $\Psi_{tx} = 0$ and $\Psi_{rx} = 0$ had no spatial

correlation but intertap correlation. The performance gap between these two channels was 1.1 dB at BER=10^{-4}. As the transmit correlation or receive correlation increases on top of the intertap correlation, the BER performance becomes worse. At the extreme case of $\Psi_{tx} = 0.9$ and $\Psi_{rx} = 0.9$, the BER performance was about 4 dB worse than that of no spatial correlation, or 5 dB worse than that of the i.i.d. channel.

3.5. Conclusion

In this paper the effects of spatial correlation on the BER are analyzed. The results show that the BER is relatively unaffected by a reduction in receivers as long as the aperture is the same. A correlation matrix was decomposed into an estimated Kronecker product and the error between the original matrix and the estimated Kronecker product was quantified. Simulations with differing amounts of spatial and iter-tap correlation were conducted. The simulation and experimental results show that the BER of MIMO systems with high spatial correlation is worse than systems with low spatial correlation.

3.6. Acknowledgment

This work was supported in part by the National Science Foundation under Grant ECCS-0846486 and the Office of Naval Research under Grants N00014-10-1-0174. The authors are grateful to Dr. J. Preisig for his leadership of conducting the SPACE08 experiments.

References

[1] C. Xiao, J. Wu, S.-Y. Leong, Y. R. Zheng, and K. B. Letaief, A discretetime model for triply selective MIMO Rayleigh fading channels, *IEEE Trans. Wireless Commun.*, vol. 3, no. 5, pp. 16781688, Sept. 2004.

[2] M. Herdin, N. Czink, H. Özcelik, E. Bonek, "Correlation Matrix Distance, a Meaningful Measure for Evaluation of Non-Stationary MIMO Channels," *IEEE VTC 2005.*

[3] J. Zhang, Y. R. Zheng, and C. Xiao, "Frequency-domain turbo equalization for MIMO underwater acoustic communications," in *Proc. IEEE OCEANS'09*, Bremen, Germany, May 11-14, 2009.

[4] W. Yang and T. C. Yang, "High frequency channel characterization for M-ary frequency-shift keying underwater acoustic communications," *J. Acoust. Soc. Am.*, vol.120, pp.2615-2626, Nov. 2006.

[5] J. Zhang, J. Cross, and Y.R. Zheng, "Statistical Channel Modeling of Wireless Shallow Water Acoustic Communications from Experiment Data," *IEEE Intl. Conf. Military Communications* (Milcom), San Jose, CA, Nov. 2010.

[6] A. G. Zajic', "Statistical modeling of MIMO mobile-to-mobile underwater channels," IEEE GLOBECOM 2010, Miami, FL, Dec. 6-10, 2010.

[7] M. Chitre, "A high-frequency warm shallow water acoustic communications channel model and measurements," *J. Acoust. Soc. America*, vol.122, pp.2580-2586.

[8] T. C. Yang, "Correlation-based decision-feedback equalizer for underwater acoustic communications," *IEEE J. Ocean Eng.*, vol.30, pp.865-880, Oct. 2005.

SECTION

2. CONCLUSIONS

Statistical characteristics, including PDF and second-order statistics, for the UWA channels measured from experimental data are analyzed. Experimental results demonstrate that the real and imaginary parts of the complex UWA channels do not follow Gaussian; the PDF of the magnitude fits the compound K distribution; the PDF of phase approximately follows uniform distribution. The autocorrelations of CIRs behave like decaying exponential curves and the channel coherence time is also roughly estimated. The scattering function provides better understanding on the spectral density of the UWA channels. Effects of spatial correlation on the BER are also analyzed. It is shown that the BER is relatively unaffected by a reduction in receivers as long as the aperture is the same. Experimental results show that the BER of MIMO systems with high spatial correlation is worse than systems with low spatial correlation. Simulations with differing amounts of spatial and iter-tap correlation were conducted verifying the experimental results.

VITA

Jesse Cross was born in Saint Louis, Missouri. He received his Bachelor's in Electrical Engineering in May 2010 at Missouri University of Science and Technology. He held an undergraduate research position under Dr. Rosa Zheng from June 2007 to May 2010 and a graduate research position from June 2010 to December 2011. He received a Chancellor's Fellowship from June 2010 to December 2011. He had internships at Hunter Engineering, Dynetics, and Sandia National Laboratories. He published three papers, two in MILCOM and one in the Navy Journal of Underwater Acoustics. He is expected to receive a Master's in Electrical Engineering at Missouri University of Science and Technology in December, 2011.